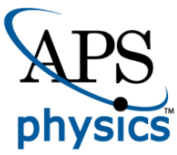

Thermal Transport Signatures of Broken-Symmetry Phases in Graphene

Falko Pientka, Jonah Waissman, Philip Kim, and Bertrand I. Halperin

Phys. Rev. Lett. **119**, 027601 — Published 14 July 2017

DOI: 10.1103/PhysRevLett.119.027601

Thermal Transport Signatures of Broken-Symmetry Phases in Graphene

Falko Pientka,[1] Jonah Waissman,[1] Philip Kim,[1] and Bertrand I. Halperin[1]

[1]*Department of Physics, Harvard University, Cambridge, Massachusetts 02138, USA*

In the half-filled zero-energy Landau level of bilayer graphene, competing phases with spontaneously broken symmetries and an intriguing quantum critical behavior have been predicted. Here we investigate signatures of these broken-symmetry phases in thermal transport measurements. To this end we calculate the spectrum of spin and valley waves in the $\nu = 0$ quantum Hall state of bilayer graphene. The presence of Goldstone modes enables heat transport even at low temperatures, which can serve as compelling evidence for spontaneous symmetry breaking. By varying external electric and magnetic fields, it is possible to determine the nature of the symmetry breaking. Temperature-dependent measurements may yield additional information about gapped modes.

Introduction.—The zero-energy Landau level of bilayer graphene has emerged as an intriguing experimental platform to study interaction-induced spontaneous symmetry breaking and competing orders. Following early theoretical work on quantum Hall ferromagnetism in graphene [1–12], several experiments have gathered evidence for a rich phase diagram of integer and fraction quantum Hall states in monolayer and bilayer graphene [13–23]. Of particular interest are the $\nu = 0$ states, where short-range interactions on the lattice scale may lead to the formation of insulating phases and spontaneous symmetry breaking of spin or isospin (valley) degrees of freedom [24, 25]. Indeed, experimental observations based on electrical transport and capacitive measurements [18, 19, 23] seem consistent with the phase diagram proposed in Refs. [24, 25], however, direct evidence for spontaneous symmetry breaking remains elusive.

As an alternative approach to charge based measurements, we propose to study broken-symmetry phases in the $\nu = 0$ quantum Hall state of bilayer graphene by thermal transport. At low temperatures, certain phases with spontaneous symmetry breaking can support heat flow via gapless spin or isospin waves, whereas heat conduction is blocked in phases without spontaneous order and a gapped spectrum of collective excitations. Hence thermal transport can yield direct evidence for spontaneous symmetry breaking and provide detailed information about collective modes. The technique is complementary to previous experiments as it is sensitive to both spin and isospin degrees of freedom and addresses insulating samples. In a broader context, thermal transport in graphene has recently been applied to study the breakdown of Fermi liquid behavior [26] as well as exotic electron-phonon scattering mechanisms [27, 28].

A possible experimental setup is shown in Fig. 1(a). A graphene bilayer is contacted by leads at different temperatures, which can be measured separately as in recent experiments [28–31]. A strong perpendicular magnetic field drives the system into a quantum Hall regime and induces a Zeeman energy ϵ_Z. The magnitude of ϵ_Z can be tuned independently by an additional in-plane field, as the interactions in graphene quantum-Hall states only

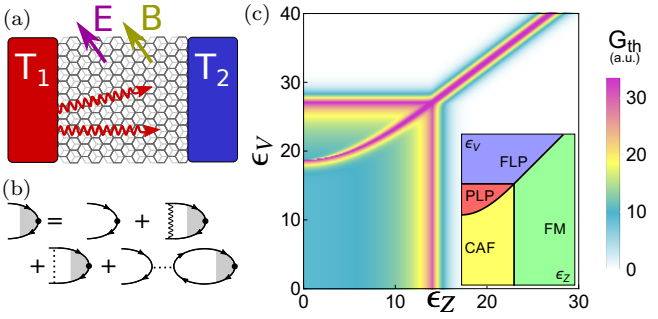

FIG. 1: (a) Experimental setup: bilayer graphene in perpendicular magnetic and electric fields between two metallic leads. (b) Diagrammatic representation of the vertex function $\Gamma_{A,ab}$ comprising the Fock contribution of the long-range Coulomb interaction (wavy line) and Hartree and Fock contributions of the anisotropic short-range interaction (dotted line). (c) Thermal conductance from particle-hole excitations at $T = 1\,\mathrm{K}$ as a function of Zeeman energy and displacement field [32]. Inset: phase diagram of the $\nu = 0$ state in bilayer graphene. The axes are the same as in the main plot.

depend on the perpendicular component. A perpendicular electric field induces a displacement field ϵ_V between the two layers. In the zero-energy Landau level, the layers are coupled to the isospin index and thus $\epsilon_{Z/V}$ control the spin (isospin) polarization. Before introducing our model we briefly outline the central result of our work. Figure 1(c) shows the contribution to the low-temperature thermal conductance G_{th} from collective modes as a function of ϵ_Z and ϵ_V. Comparison with the phase diagram in the inset reveals that thermal transport exhibits clear signatures of spontaneous symmetry breaking. Heat can flow via Goldstone modes inside the canted antiferromagnet (CAF) or partially-layer polarized (PLP) phase due to spontaneously broken spin or isospin symmetries. In contrast, the thermal conductance from collective modes vanishes in the fully layer polarized (FLP) and ferromagnetic (FM) phases, where the excitation spectrum is gapped [32]. Moreover G_{th} is dramatically enhanced near phase transitions, due to the large low-energy density of states of gapless quadratic modes present at the critical points.

Model.—We follow Refs. [24, 25] to describe symmetry breaking in the lowest Landau level of bilayer graphene in the Hartree–Fock approximation. We assume a large Landau level spacing and project onto the lowest Landau level. The bare Coulomb interactions can be strongly renormalized by Landau level mixing even at strong fields [24]. Instead we assume renormalized parameters which are determined from experiment.

The zero-energy Landau level of bilayer graphene is eightfold degenerate [1]. The states are annihilated by operators $c_{a,k}$ with index $a = \{n_a, \alpha\}$ combining orbital index $n_a = 0, 1$ and SU(4) index α that accounts for spin and isospin. We shall use the basis $\Psi_a(\mathbf{r}) = \sum_k \langle \mathbf{r}|\psi_{a,k}\rangle\, c_{a,k}$, where $|\psi_{a,k}\rangle = \chi_\alpha\, |n_a, k\rangle$ with χ_α an SU(4) spinor and $|n, k\rangle$ the Landau level wavefunctions.

The Hamiltonian is $H = \int d^2r \Psi_a^\dagger(\mathbf{r}) \mathcal{H}_{s,\alpha} \Psi_a(\mathbf{r}) + H_i$, where $\mathcal{H}_s = -\epsilon_Z \sigma_z - \epsilon_V \tau_z$ is the single-particle term, σ_j (τ_j) are Pauli matrices in spin (isospin) space, and $H_i = (1/2)\sum_{abcd} \int d^2r d^2r' \Psi_a^\dagger(\mathbf{r}) \Psi_b^\dagger(\mathbf{r}') \Psi_c(\mathbf{r}') \Psi_d(\mathbf{r}) V_{\alpha\beta\gamma\delta}(\mathbf{r} - \mathbf{r}')$ with $V_{\alpha\beta\gamma\delta}(\mathbf{r}) = (e^2/\epsilon r)\delta_{\alpha\delta}\delta_{\beta\gamma} + \delta(\mathbf{r}) W_{\alpha\beta\gamma\delta}$ describes Coulomb interactions. Introducing the parameters $u_x = u_y = u_\perp$ and u_z the short-range contribution can be expressed as $W_{\alpha\beta\gamma\delta} = \pi l_B^2 \sum_{j=x,y,z} u_j (\tau_j)_{\alpha\delta} (\tau_j)_{\beta\gamma}$, with l_B the magnetic length [24, 25]. Our model neglects terms of higher order in the interaction which break the U(1) isospin symmetry down to a discrete C_3 symmetry due to the lattice structure of graphene.

Guided by experiment [33], we shall use the following parameters appropriate for a perpendicular magnetic field of $B_\perp = 5\mathrm{T}$: $\epsilon_Z = 3\,\mathrm{K}$ (Figs. 2 and 3), $u_\perp = -7\,\mathrm{K}$, $u_z = 20\,\mathrm{K}$, and $U_c = 100\,\mathrm{K}$. Assuming a sample width of $W = 5\,\mu\mathrm{m}$, we estimate a thermal conductance of the Goldstone mode in the CAF phase of $G_{\mathrm{th}} = 17\,\mathrm{pW/K}$ at $T = 1\,\mathrm{K}$ [33], which is accessible in experiment [28].

Excitations within the $\nu = 0$ Landau level.—We calculate the spectrum of intra-Landau-level particle-hole excitations following Ref. [34] from the response to an operator θ_A in SU(4) spin space

$$\chi_A(\mathbf{k},\omega) = \sum_{ab} \sum_{q_1,q_2} \langle q_1 a|e^{i\mathbf{kr}} \theta_A^\dagger |q_2 b\rangle \times \int \frac{d\omega'}{2\pi} G_a(\omega+\omega') G_b(\omega') \Gamma_{A,ab}(q_1, q_2; \mathbf{k}, \omega), \quad (1)$$

where the vertex part Γ_A is given by the diagrams shown in Fig. 1(b). The excitation spectrum can be found from the poles of the response function χ_A. A tedious but straightforward calculation [33] yields the equation

$$\sum_{cd} [\delta_{ac}\delta_{bd}[(f_c - f_d)\omega - E_{\mathrm{xc},cd}] - \tilde{V}_{abcd}(\mathbf{k})] B_{cd} = 0, \quad (2)$$

where E_{xc} is the exchange energy, which accounts for single-particle and self energy contributions, and $\tilde{V}_{abcd}$ denotes interaction matrix elements comprising Hartree and Fock contributions [33]. This equation has to be satisfied for all pairs (a, b) and (c, d) with one occupied and one empty state. In the limit of large Coulomb energy $U_c' = N_0 U_c \gg u_\perp, u_z$, with $U_c = \sqrt{\pi/2}(e^2/\epsilon l_B)$ and $N_0 = 89/224$, fluctuations of the orbital index n are suppressed [4, 10] and at low energies the resulting 32×32 eigenvalue problem can be further reduced [33] to an 8×8 problem. Incidentally, the resulting eigenvalue equation has the same analytical form as for monolayer graphene when $\epsilon_V = 0$ and $N_0 = 1/4$. Hence, our results can also be applied to monolayers (see also [35]).

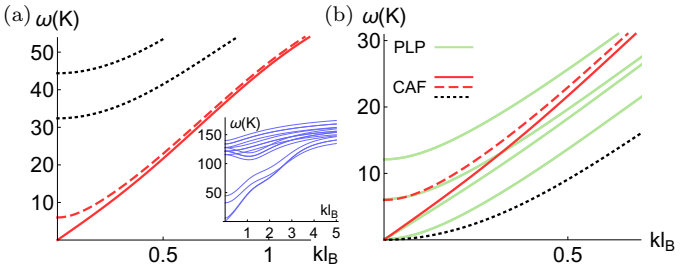

FIG. 2: (a) Excitation spectrum in the CAF phase for $\epsilon_V = 3\,\mathrm{K}$. The two low-energy modes (red solid and dashed) are spin waves at low wavevectors, while the higher-energy modes (black dotted) correspond to isospin fluctuations. Inset: full spectrum with energies up to $\sim U_c$. (b) Excitation spectrum at $\epsilon_V = 19.2 \pm 0.1\,\mathrm{K}$ on the two sides of the CAF–PLP transition. We use the same color coding as in (a) for the spectrum on the CAF side and green solid lines on the PLP side.

The 8×8 matrix can be readily diagonalized and we obtain four low-energy modes along with their particle-hole symmetric partners. We expand the spectrum at long wavelength, $kl_B \ll 1$, and find in the CAF phase, where $u_\perp < 0$,

$$\omega_1 \simeq vk, \qquad v = 2l_B \sin\theta_s \sqrt{|u_\perp| U_c'}, \quad (3)$$

$$\omega_2 \simeq 2\epsilon_Z + k^2 l_B^2 U_c' (\epsilon_Z^2 + 4u_\perp^2)/4|u_\perp|\epsilon_Z, \quad (4)$$

$$\omega_{3,4} \simeq \Delta_c \mp 2\epsilon_V + k^2 l_B^2 U_c' (\epsilon_Z + 4|u_\perp|u_z)/2|u_\perp|\Delta_c \quad (5)$$

with $\Delta_c^2 = 4(u_z + |u_\perp|)(u_z - |u_\perp| + \epsilon_Z^2/2|u_\perp|)$. The spectrum is shown in Fig. 2(a). We find a gapless mode in agreement with the spontaneously broken $U(1)$ spin symmetry in the CAF phase and the next higher mode with a gap of $2\epsilon_Z$, which corresponds to spin fluctuations along the Zeeman field direction. The velocity of the Goldstone mode depends on the canting angle $\cos\theta_s = \epsilon_Z/2|u_\perp|$. The higher modes $\omega_{3/4}$ are associated with isospin fluctuations.

Increasing the Zeeman field polarizes the spins along the field direction until the system enters the FM phase when $\theta_s = 0$ and the velocity of the Goldstone mode vanishes. The gapless modes thus becomes quadratic at the critical point and a gap opens as the system enters the FM phase [33] and spin fluctuations around the Zeeman field direction are further suppressed by an increasing field strength.

If, instead, we increased the displacement field ϵ_V, the

CAF phase transitions into the PLP phase when $\epsilon_V = \Delta_c/2$ [25]. At this point the quadratic mode ω_3 is gapless in addition to ω_1. Interestingly the excitation spectrum is discontinuous at the critical point reflecting the first-order nature of this transition. The spectrum in the PLP phase for $kl_B \ll 1$ is given by [33]

$$\omega_1 \simeq vk,\ v \simeq l_B \sin\theta_m \sqrt{2U_c'(u_z + |u_\perp|)}, \quad (6)$$

$$\omega_2 \simeq \Delta_p + k^2 l_B^2 U_c'[(u_z + |u_\perp|)\sin^2\theta_m - 4|u_\perp|]/\Delta_p, \quad (7)$$

and $\omega_{3,4} = \omega_2 \mp 2\epsilon_Z$. Here we have introduced the canting angle of the isospin $\cos\theta_m = \epsilon_V/(u_z + |u_\perp|)$ and $\Delta_p^2 = 8|u_\perp|(\epsilon_V^2 + u_\perp^2 - u_z^2)/(u_z + |u_\perp|)$. The PLP phase features a Goldstone mode ω_1 due to the broken U(1) symmetry in the isospin sector, along with several gapped modes. If the CAF–PLP transition is approached from the PLP side, ω_3 becomes gapless. The spectra on the CAF and PLP side of the transition are compared in Fig. 2(b). The three lowest modes coincide in both phases at $k = 0$, but have different dispersions. Interestingly, another low-energy mode with a gap of $4\epsilon_Z = 12\,\mathrm{K}$ is present in the PLP phase. In contrast, the fourth mode in the CAF is shifted to much higher energies, $4\epsilon_V \simeq 77\,\mathrm{K}$.

Further increasing ϵ_V leads to a stronger polarization of the isospins and the system enters the FLP phase once $\theta_m = 0$. This transition is continuous and the gapless mode becomes quadratic at the critical point similar to the CAF–FM transition. On the FLP side this mode acquires a gap, which grows with increasing displacement field as isospin fluctuations are suppressed [33].

Thermal conductance.—Thermal transport at low temperatures can indicate the presence of neutral low-energy excitations. Importantly, the broken-symmetry phases CAF and PLP support thermal transport via Goldstone modes and can thus be readily distinguished from phases with a gapped spectrum and exponentially suppressed thermal conductance at low temperatures. In order to relate the thermal conductance to the presence of particle-hole excitations we must rule out other origins of heat transport, most importantly, electrons and phonons.

At low temperatures we can safely ignore electronic heat transport in the insulating phases CAF, PLP, and FLP [36]. While the FM phase is also insulating in the bulk, it has conducting edge states [18, 19], which could contribute to heat transport. The electronic contribution is linear in T and can be considerably smaller than the bulk conductance in the CAF phase $\propto T^2$ [37]. An electronic heat current can in principle be suppressed by measuring in a Corbino geometry [38] or by adding side leads acting as heat sinks for the edge states.

Heat transport via phonons in nonsuspended samples can presumably be neglected in the setup of Fig. 1(a). Phonons will thermalize with the substrate before reaching the drain and thus energy transfered to phonons is lost. We expect such losses to be small at low temperatures due to the high power-law decay of the electron-phonon energy relaxation rate $\propto T^4$ in graphene [27, 30].

In the following, we focus on the heat current carried by particle-hole excitations and ignore other contributions. We model the leads as black bodies assuming sufficiently rough interfaces between leads and sample. We furthermore assume ballistic transport through the sample ignoring defects and scattering between SU(4) spin waves. Ballistic transport of magnons on a millimeter scale has been observed in the three-dimensional antiferromagnet Nd_2CuO_4 [39]. In contrast, earlier works on quasi-two-dimensional antiferromagnets found typical mean free paths of $\sim 100\,\mathrm{nm}$ attributed to scattering off defects [40–42]. However, it is reasonable to assume a considerably longer scattering length in high-quality graphene samples, where such defects are not present. The magnon-magnon scattering rate in a two dimensional antiferromagnet for modes with $vk \sim T$ is $\sim vk(T/2\pi\rho)^2$ [43], where $\rho \sim U_c'$ is the spin stiffness. In the CAF phase at $T = 10\,\mathrm{K}$ this yields a magnon-magnon scattering length of several microns.

In two-dimensions the heat current through a medium of width W with an isotropic dispersion $\omega(k)$ is given by [44] $J = (W/2\pi^2)\int dk\, k\omega(k)v_k n_B[\omega(k)]$, where $v_k = \partial_k\omega(k)$ and $n_B(\omega)$ is the Bose distribution. Assuming the sample to be much longer than the thermal wavelength ($\lambda \sim 300\,\mathrm{nm}$ at $T = 1\,\mathrm{K}$ [33]), we can neglect evanescent modes and resonances. We then obtain the thermal conductance as $G_{\mathrm{th}} = (J_L - J_R)/\Delta T$ where $J_{L/R}$ are the heat currents from the left and right reservoir with temperature $T_{L/R}$ and $\Delta T = |T_L - T_R| \ll T_L$.

The thermal conductance of the different phases can be compared in a single sample by tuning ϵ_V via a gate voltage and ϵ_Z by an in-plane magnetic field. Figure 1(c) shows the thermal conductance at $T = 1\,\mathrm{K}$ along with the corresponding phase diagram in the inset. The phases with broken symmetries, CAF and PLP, exhibit thermal transport, whereas the conductance is exponentially suppressed inside the gapped phases, FLP and FM.

The phase transitions give rise to particularly strong signatures in thermal transport. At the first-order CAF–PLP transition a mode with a quadratic dispersion becomes gapless in addition to the linear Goldstone modes present in both phases [cf. Fig. 2(b)]. Thus once the energy minimum of the quadratic mode becomes comparable to temperature, the available phase space for heat conduction increases dramatically. The continuous transition between PLP and FLP does not involve any additional low-energy modes, but the linear dispersion of the gapless mode in the PLP phase becomes quadratic at the critical point. The large density of states at the bottom of the quadratic band causes G_{th} to peak at the transition.

We emphasize that all phase transitions have prominent signatures in the thermal conductance. This constitutes an important result of our work. While previous experiments based on charge transport have iden-

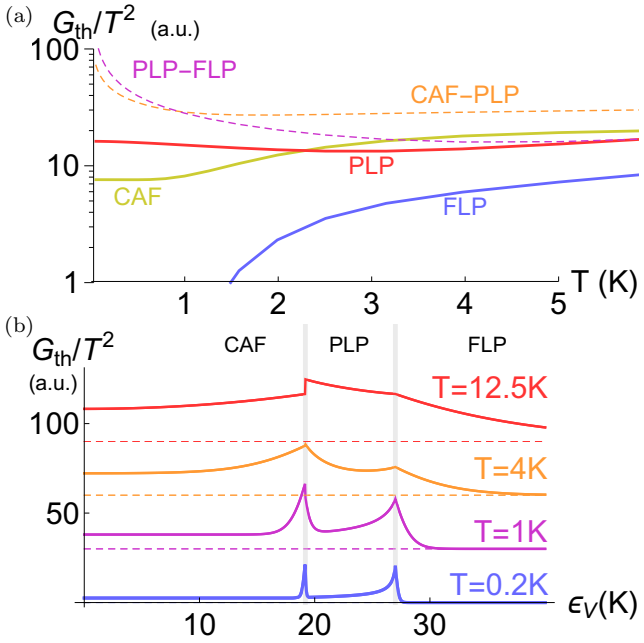

FIG. 3: (a) Thermal conductance normalized by T^2 inside the three phases CAF, PLP, and FLP at $\epsilon_V = 15\,\mathrm{K}$, $25\,\mathrm{K}$, $31\,\mathrm{K}$ (solid lines) as well as near the phase transitions CAF–PLP and PLP–FLP at $\epsilon_V = 19.21\,\mathrm{K}$, $27\,\mathrm{K}$ (dashed lines). (b) Thermal conductance *vs* ϵ_V for various temperatures. Curves have been offset for clarity (the dashed lines indicate zero conductance) and the vertical gray lines mark the phase transitions.

tified phase boundaries [14, 16, 18] it remains unclear which transitions should exhibit signatures in such experiments [45, 46]. Thus thermal transport measurements could possibly lead to the discovery of previously unresolved phase transitions. Moreover, they could determine whether the layer-polarized state observed in experiment is a broken-symmetry PLP state or a gapped FLP state.

While low-temperature measurements are sufficient to determine the phase diagram, more detailed information about the excitation spectrum can be gained by varying temperature. The conductance of a linear dispersion, $\omega(k) = vk$, follows the Stefan–Boltzmann law in two dimensions $G_{\mathrm{th}} \sim WT^2/v$. In contrast, a gapless quadratic mode leads to a weaker power-law dependence $G_{\mathrm{th}} \propto T^{3/2}$ [33]. The conductance of a gapped spectrum is exponentially suppressed at low temperatures.

In the following we concentrate on the three electronically insulating phases CAF, PLP and FLP. Figure 3(a) shows the temperature dependence of the conductance divided by T^2 within the three phases and at the transition points. The thermal conductance in FLP shows an activated behavior from which one can extract the gap in the excitation spectrum. The conductance in the PLP phase follows approximately a T^2 law indicating that only the linear Goldstone mode has significant occupation up to a temperature of $T = 5\,\mathrm{K}$. In the CAF phase $G_{\mathrm{th}} \propto T^2$ at low temperatures $T \lesssim 1\,\mathrm{K}$ indicating a Goldstone mode. At temperatures above $3\,\mathrm{K}$ the conductance follows a T^2 law with a larger proportionality constant, which implies that additional gapped low-energy excitations become occupied above $T = 1\,\mathrm{K}$. At the critical points between CAF, PLP and FLP, the conductance increases slower than T^2 and thus G_{th}/T^2 decreases. This is a signature of gapless quadratic modes with a characteristic $T^{3/2}$ behavior. Hence the conductance peaks at phase transitions become particularly pronounced at low temperatures.

Additional information can be obtained from traces of the conductance as a function of displacement field for fixed Zeeman energy shown in Fig. 3(b). Interestingly, the signature of the CAF–PLP transition changes with temperature. A strong peak at low-temperatures turns into a pronounced discontinuity above $T = 10\,\mathrm{K}$. This clearly signals a first-order phase transition, where the excitation spectrum changes discontinuously between the two phases. The most striking difference between the spectra shown in Fig. 2(b) is an additional mode in the PLP phase with an energy minimum of $12\,\mathrm{K}$, which causes a sizable jump in the conductance. This discontinuity survives with increasing temperature until high-energy modes at around $\omega = 70\,\mathrm{K}$ get populated.

The PLP–FLP transition, in contrast, is of second-order and thus the conductance is continuous. Instead, the derivative of the conductance with respect to ϵ_V jumps at the critical point, signaling a higher-order phase transition. The FLP phase shows activated transport whose activation energy grows with distance from the critical point. This is a clear signature of the FLP phase where the gap increases with layer polarization.

The conductance as a function of displacement field can distinguish CAF and PLP phases and clarify the character of the gapless modes. In the CAF phase the lowest-energy excitations are spin waves, which leave the mean isospin polarization unchanged. Hence the Goldstone mode velocity does not depend on the displacement field which acts only on isospin degrees of freedom and the conductance remains constant in a broad range of fields. In the PLP phase the Goldstone mode is an isospin wave and hence its velocity decreases with ϵ_V in agreement with Eq. (6). Consequently, the thermal conductance grows when increasing ϵ_V according to the Stefan–Boltzmann law, $G_{\mathrm{th}} \propto 1/v$. This distinctive behavior is clearly visible at $T = 0.2\,\mathrm{K}$ and $1\,\mathrm{K}$ in Fig. 3(b).

Alternatively, one can verify the magnetic nature of the Goldstone mode in the CAF phase by tuning the Zeeman field, which changes the spin-wave velocity but leaves the isospin-wave velocity in the PLP phase unchanged. Thus by tuning ϵ_V and ϵ_Z one can elucidate the nature of the broken symmetry in the ground state and the spin-isospin structure of the Goldstone modes.

Conclusions.—Low-temperature thermal transport in the $\nu = 0$ state of bilayer graphene exhibits unique signatures of various ordered phases and phase transitions.

Obtaining evidence of the CAF and PLP states would be particularly intriguing as the first-order transition between these states closely resembles the antiferromagnet–superconductor transition in some high T_c superconductors [35, 45, 47] and may exhibit deconfined quantum criticality [48]. It would be interesting to extend this work to study other insulating phases in two dimensions such as in moiré heterostructures [49]. Another exciting future direction is to study the bulk thermal transport of broken-symmetry quantum Hall states at other filling factors which could possibly be achieved in a Corbino geometry.

During the final stages of this work we became aware of Ref. [50] which also calculates the excitation spectrum of bilayer graphene.

We acknowledge financial support by the STC Center for Integrated Quantum Materials, NSF Grant No. DMR-1231319.

[1] E. McCann and V. I. Fal'ko, Phys. Rev. Lett. **96**, 086805 (2006), URL http://link.aps.org/doi/10.1103/PhysRevLett.96.086805.

[2] K. Yang, S. Das Sarma, and A. H. MacDonald, Phys. Rev. B **74**, 075423 (2006), URL http://link.aps.org/doi/10.1103/PhysRevB.74.075423.

[3] I. L. Aleiner, D. E. Kharzeev, and A. M. Tsvelik, Phys. Rev. B **76**, 195415 (2007), URL http://link.aps.org/doi/10.1103/PhysRevB.76.195415.

[4] Y. Barlas, R. Côté, K. Nomura, and A. H. MacDonald, Phys. Rev. Lett. **101**, 097601 (2008), URL http://link.aps.org/doi/10.1103/PhysRevLett.101.097601.

[5] D. A. Abanin, S. A. Parameswaran, and S. L. Sondhi, Phys. Rev. Lett. **103**, 076802 (2009), URL http://link.aps.org/doi/10.1103/PhysRevLett.103.076802.

[6] Y. Barlas, R. Côté, J. Lambert, and A. H. MacDonald, Phys. Rev. Lett. **104**, 096802 (2010), URL https://link.aps.org/doi/10.1103/PhysRevLett.104.096802.

[7] Y. Lemonik, I. L. Aleiner, C. Toke, and V. I. Fal'ko, Phys. Rev. B **82**, 201408 (2010), URL http://link.aps.org/doi/10.1103/PhysRevB.82.201408.

[8] Y. Lemonik, I. Aleiner, and V. I. Fal'ko, Phys. Rev. B **85**, 245451 (2012), URL http://link.aps.org/doi/10.1103/PhysRevB.85.245451.

[9] R. Nandkishore and L. Levitov, Physica Scripta **2012**, 014011 (2012), URL http://stacks.iop.org/1402-4896/2012/i=T146/a=014011.

[10] K. Shizuya, Phys. Rev. B **86**, 045431 (2012), URL http://link.aps.org/doi/10.1103/PhysRevB.86.045431.

[11] B. Roy, Phys. Rev. B **89**, 201401(R) (2014), URL https://link.aps.org/doi/10.1103/PhysRevB.89.201401.

[12] A. Knothe and T. Jolicoeur, Phys. Rev. B **94**, 235149 (2016), URL http://link.aps.org/doi/10.1103/PhysRevB.94.235149.

[13] B. E. Feldman, J. Martin, and A. Yacoby, Nat Phys **5**, 889 (2009), URL http://dx.doi.org/10.1038/nphys1406.

[14] R. T. Weitz, M. T. Allen, B. E. Feldman, J. Martin, and A. Yacoby, Science **330**, 812 (2010), URL http://science.sciencemag.org/content/330/6005/812.

[15] J. Martin, B. E. Feldman, R. T. Weitz, M. T. Allen, and A. Yacoby, Phys. Rev. Lett. **105**, 256806 (2010), URL http://link.aps.org/doi/10.1103/PhysRevLett.105.256806.

[16] J. Velasco, L. Jing, W. Bao, Y. Lee, P. Kratz, V. Aji, M. Bockrath, C. N., Lau, C. Varma, R. Stillwell, et al., Nat Nano **7**, 156 (2012), URL http://dx.doi.org/10.1038/nnano.2011.251.

[17] A. F. Young, C. R. Dean, L. Wang, H. Ren, P. Cadden-Zimansky, K. Watanabe, T. Taniguchi, J. Hone, K. L. Shepard, and P. Kim, Nat Phys **8**, 550 (2012), URL http://dx.doi.org/10.1038/nphys2307.

[18] P. Maher, C. R. Dean, A. F. Young, T. Taniguchi, K. Watanabe, K. L. Shepard, J. Hone, and P. Kim, Nat Phys **9**, 154 (2013), URL http://dx.doi.org/10.1038/nphys2528.

[19] A. F. Young, J. D. Sanchez-Yamagishi, B. Hunt, S. H. Choi, K. Watanabe, T. Taniguchi, R. C. Ashoori, and P. Jarillo-Herrero, Nature **505**, 528 (2014), URL http://dx.doi.org/10.1038/nature12800.

[20] K. Lee, B. Fallahazad, J. Xue, D. C. Dillen, K. Kim, T. Taniguchi, K. Watanabe, and E. Tutuc, Science **345**, 58 (2014), URL http://science.sciencemag.org/content/345/6192/58.

[21] P. Maher, L. Wang, Y. Gao, C. Forsythe, T. Taniguchi, K. Watanabe, D. Abanin, Z. Papić, P. Cadden-Zimansky, J. Hone, et al., Science **345**, 61 (2014), URL http://science.sciencemag.org/content/345/6192/61.

[22] A. Kou, B. E. Feldman, A. J. Levin, B. I. Halperin, K. Watanabe, T. Taniguchi, and A. Yacoby, Science **345**, 55 (2014), URL http://science.sciencemag.org/content/345/6192/55.

[23] B. M. Hunt, J. I. A. Li, A. A. Zibrov, L. Wang, T. Taniguchi, K. Watanabe, J. Hone, C. R. Dean, M. Zaletel, R. C. Ashoori, et al., ArXiv e-prints (2016), 1607.06461.

[24] M. Kharitonov, Phys. Rev. B **85**, 155439 (2012), URL http://link.aps.org/doi/10.1103/PhysRevB.85.155439.

[25] M. Kharitonov, Phys. Rev. Lett. **109**, 046803 (2012), URL http://link.aps.org/doi/10.1103/PhysRevLett.109.046803.

[26] J. Crossno, J. K. Shi, K. Wang, X. Liu, A. Harzheim, A. Lucas, S. Sachdev, P. Kim, T. Taniguchi, K. Watanabe, et al., Science (2016), URL http://science.sciencemag.org/content/early/2016/02/10/science.aad0343.

[27] A. C. Betz, S. H. Jhang, E. Pallecchi, R. Ferreira, G. Feve, J.-M. Berroir, and B. Placais, Nat Phys **9**, 109 (2013), URL http://dx.doi.org/10.1038/nphys2494.

[28] K. C. Fong, E. E. Wollman, H. Ravi, W. Chen, A. A. Clerk, M. D. Shaw, H. G. Leduc, and K. C. Schwab, Phys. Rev. X **3**, 041008 (2013), URL http://link.aps.org/doi/10.1103/PhysRevX.3.041008.

[29] K. C. Fong and K. C. Schwab, Phys. Rev. X **2**, 031006 (2012), URL http://link.aps.org/doi/10.1103/PhysRevX.2.031006.

[30] J. Crossno, X. Liu, T. A. Ohki, P. Kim, and K. C. Fong, Applied Physics Letters **106**, 023121 (2015), http://dx.doi.org/10.1063/1.4905926, URL http://dx.doi.org/10.1063/1.4905926.

[31] F. Ghahari, H.-Y. Xie, T. Taniguchi, K. Watanabe, M. S. Foster, and P. Kim, Phys. Rev. Lett. **116**,

136802 (2016), URL https://link.aps.org/doi/10.1103/PhysRevLett.116.136802.
[32] Fig. 1(c) ignores a possible electronic contribution to $G_{\rm th}$ in the ferromagnetic phase due to conducting edge modes.
[33] See Supplemental Material.
[34] C. Kallin and B. I. Halperin, Phys. Rev. B **30**, 5655 (1984), URL http://link.aps.org/doi/10.1103/PhysRevB.30.5655.
[35] F. Wu, I. Sodemann, Y. Araki, A. H. MacDonald, and T. Jolicoeur, Phys. Rev. B **90**, 235432 (2014), URL http://link.aps.org/doi/10.1103/PhysRevB.90.235432.
[36] In Ref. [18] the transport gap in the CAF phase was estimated to be $\sim 40\,\mathrm{K}$ at $B = 14\,\mathrm{T}$.
[37] The ballistic edge states of the FM phase would contribute a thermal conductance of $4\,\mathrm{pWK}^{-2} \times T$ compared to $G_{\rm th} \simeq 17\,\mathrm{pWK}^{-3} \times T^2$ in the CAF phase in a $5\,\mu$m wide sample.
[38] Y. Zhao, P. Cadden-Zimansky, F. Ghahari, and P. Kim, Phys. Rev. Lett. **108**, 106804 (2012), URL https://link.aps.org/doi/10.1103/PhysRevLett.108.106804.
[39] S. Y. Li, L. Taillefer, C. H. Wang, and X. H. Chen, Phys. Rev. Lett. **95**, 156603 (2005), URL http://link.aps.org/doi/10.1103/PhysRevLett.95.156603.
[40] A. V. Sologubenko, E. Felder, K. Giannò, H. R. Ott, A. Vietkine, and A. Revcolevschi, Phys. Rev. B **62**, R6108 (2000), URL http://link.aps.org/doi/10.1103/PhysRevB.62.R6108.
[41] B. C. Sales, M. D. Lumsden, S. E. Nagler, D. Mandrus, and R. Jin, Phys. Rev. Lett. **88**, 095901 (2002), URL http://link.aps.org/doi/10.1103/PhysRevLett.88.095901.
[42] C. Hess, B. Büchner, U. Ammerahl, L. Colonescu, F. Heidrich-Meisner, W. Brenig, and A. Revcolevschi, Phys. Rev. Lett. **90**, 197002 (2003), URL http://link.aps.org/doi/10.1103/PhysRevLett.90.197002.
[43] S. Tyč and B. I. Halperin, Phys. Rev. B **42**, 2096 (1990), URL http://link.aps.org/doi/10.1103/PhysRevB.42.2096.
[44] J. M. Ziman, *Electrons and Phonons* (Oxford University Press, London, 1960).
[45] J. Lee and S. Sachdev, Phys. Rev. Lett. **114**, 226801 (2015), URL http://link.aps.org/doi/10.1103/PhysRevLett.114.226801.
[46] K. Dhochak, E. Shimshoni, and E. Berg, Phys. Rev. B **91**, 165107 (2015), URL http://link.aps.org/doi/10.1103/PhysRevB.91.165107.
[47] J. Lee and S. Sachdev, Phys. Rev. B **90**, 195427 (2014), URL http://link.aps.org/doi/10.1103/PhysRevB.90.195427.
[48] T. Senthil, A. Vishwanath, L. Balents, S. Sachdev, and M. P. A. Fisher, Science **303**, 1490 (2004), URL http://science.sciencemag.org/content/303/5663/1490.
[49] Y. Cao, J. Y. Luo, V. Fatemi, S. Fang, J. D. Sanchez-Yamagishi, K. Watanabe, T. Taniguchi, E. Kaxiras, and P. Jarillo-Herrero, Phys. Rev. Lett. **117**, 116804 (2016), URL http://link.aps.org/doi/10.1103/PhysRevLett.117.116804.
[50] J. R. M. de Nova and I. Zapata, ArXiv e-prints (2017), 1701.03278.